

Document downloaded from:

<http://hdl.handle.net/10251/176183>

This paper must be cited as:

Batista-Grau, P.; Sánchez Tovar, R.; Fernández Domene, RM.; Garcia-Anton, J. (2020). Formation of ZnO nanowires by anodization under hydrodynamic conditions for photoelectrochemical water splitting. *Surface and Coatings Technology*. 381:1-7. <https://doi.org/10.1016/j.surfcoat.2019.125197>



The final publication is available at

<https://doi.org/10.1016/j.surfcoat.2019.125197>

Copyright Elsevier

Additional Information

# Formation of ZnO nanowires by anodization under hydrodynamic conditions for photoelectrochemical water splitting.

P. Batista-Grau <sup>a</sup>, R. Sánchez-Tovar <sup>a,b</sup>, R.M. Fernández-Domene <sup>a</sup>, J. García-Antón <sup>a\*</sup>

<sup>a</sup> *Ingeniería Electroquímica y Corrosión (IEC), Instituto Universitario de Seguridad Industrial, Radiofísica y Medioambiental (ISIRYM), Universitat Politècnica de València, Camino de Vera s/n, 46022 Valencia, Spain. \* [jgarciaa@iqn.upv.es](mailto:jgarciaa@iqn.upv.es)*

<sup>b</sup> *Departamento de Ingeniería Química, Universitat de València, Av de les Universitats, s/n, 46100 Burjassot, Spain.*

## Abstract

The present work studies the influence of hydrodynamic conditions (from 0 to 5000 rpm) during Zn anodization process on the morphology, structure and photoelectrocatalytic behavior of ZnO nanostructures. For this purpose, analysis with Confocal Laser-Raman Spectroscopy, Field Emission Scanning Electron Microscope (FE-SEM) and photoelectrochemical water splitting tests were performed. This investigation reveals that hydrodynamic conditions during anodization promoted the formation of ordered ZnO nanowires along the surface that greatly enhance its stability and increases the photocurrent density response for water splitting in a 159 % at the 5000 rpm electrode rotation speed.

**Keywords:** zinc oxide, anodization, hydrodynamic conditions, bicarbonate, photoelectrocatalyst, water splitting.

## 1. Introduction

Zinc oxide is a n-type semiconductor [1–3] that presents wurtzite hexagonal structure [1]. Without doping, its semiconductor properties are due to oxygen vacancies and/or zinc interstitial defects [1]. Its wide band gap of 3.37 eV [1–7] allows the absorption of light in the UV region [5]. Moreover, it presents a high exciton binding energy of 60 meV at room temperature [1–3,6–8] that is much larger than for other semiconductor materials [6]; and a high electron mobility ( $205\text{--}1000\text{ cm}^2\text{ V}^{-1}\text{ s}^{-1}$ ) [5], from 10 to 100 times higher compared to titanium dioxide [9], which provides large electrical conductivity and makes ZnO a better candidate as a photoanode [10]. In addition, it has a high electrochemical coupling coefficient [7], thermal stability [1,6], high photostability [7], low-cost [11], low toxicity [7,12,13] and biodegradability [14]. All these properties make zinc oxide a promising material for several applications, including catalysis [5], photocatalysis [2,3,6,12], photovoltaics [3], solar cells [2,5,6,11,12,15–18], photoelectrochemical (PEC) water splitting for hydrogen generation [11,17], ultraviolet (UV) light-emitting diodes [2,3,6,15,18], ultraviolet lasers [6,12], sensing [2,3,5,6,11,12,14], and so on.

ZnO can be obtained in the form of different structures that strongly influence its properties [6]. These can be one-dimensional (e.g. nanotubes, nanowires) , two-dimensional (e.g. nanosheet, nanopellets) and three-dimensional (e.g. flower, snowflakes) structures [7]. Among them, one-dimensional nanostructures presents particular advantages as a photocatalyst [19] with a remarkably high surface-to-volume ratio [3,14,19] that increases the active area of light absorption and interaction with the electrolyte [19], and the quantum confinement effects in which the electrons only move along the axis of the one-dimensional nanostructures [1] and consequently, enhance electron transport efficiency [3,17,20].

Until now, several effective methods to prepare ZnO nanostructures have been used: hydrothermal methods [2,4–6,11,14,15], thermal evaporation [6], chemical vapour deposition (CVD) [2,4–6,14,20], pulsed laser deposition (PLD) [2,14], molecular beam epitaxy (MBE) [2,6], template-assisted methods [2,15], metal organic chemical vapor deposition (MOCVD) [6], atomic layer deposition (ALD) [5], sol–gel chemistry [5,11], ultra-fast microwave method [15], sputtering [4,11] and electrochemical methods [2,3,5,6,14]. Most of the aforementioned strategies required high temperature growth environment [20], costly experimental setups [2,20], long reaction times [2,20] and complicated procedures [2]. In this context, electrochemical methods seem to be very promising as they are relatively low cost [2,3,6,11], fast [2,3,6] and allow large-scale synthesis [2,11]. Among them, anodization of Zn has been proposed as an efficient method for the rapid synthesis of ZnO nanowires [2,3] with the advantage of allowing the growth of the nanostructures directly on the metal substrate, which in turn would act as the back contact of the photoanode [9,19]. A problem with zinc oxide is that it presents instability in acidic electrolytes, which are generally used during anodization [5]. Bicarbonate solutions seem to be one of the most interesting alternatives among the electrolytes that have been studied for the anodization of Zn, as they allow a rapid formation of the high aspect ratio of the ZnO nanowires under mild conditions [2].

Based on previous studies [2,3,5,16,20] that have been successful in the formation of different ZnO nanostructures and the elucidation they offer in the mechanism of its growth in NaHCO<sub>3</sub> solutions, anodizing conditions such time, potential and electrolyte concentration, as well as annealing temperature and duration have been set in the present work. Potential was fixed in 10 V since it was reported to be the most optimal anodizing potential by Zaraska et al.[2]. Some authors used 5 mM NaHCO<sub>3</sub> electrolyte achieving nanowires [3,16], nevertheless Mah et al. [20] reported that generally, the diameter

average of the synthesized nanoflower (from which nanowires grew) decreased with increasing the electrolyte concentration. Therefore, high concentrations are desired to increase nanostructures surface to volume ratio. In this line, Faid et al.[21], as well as Mah et al.[20] reported the formation of nanowires in 50 mM NaHCO<sub>3</sub> electrolytes. For the anodization time, a higher growth rate is expected because of hydrodynamic conditions [2], therefore a time of 10 min was selected. Concerning the thermal treatment, Zaraska et al. [3] studied 100-300 °C annealing temperatures and determined hydrozincate-containing product was formed directly during anodization and could be easily converted to hexagonal wurtzite ZnO by thermal annealing in air at temperatures higher than 150 °C. Besides, it was determined that the average crystallite size increases with increasing annealing temperature [3]. Consequently, in this work annealing is carried out at 300 °C during 1 h.

The mentioned studies were carried out anodizing under stagnant conditions except in the case reported by Zaraska et al. [2] in which the anodization was performed with and without agitation by stirring the electrolyte. In previous researches it was demonstrated that the morphology of TiO<sub>2</sub> [22] and ZnO/ZnS heterostructures [9] was strongly influenced by controlled hydrodynamic conditions (stirring the electrode instead of the electrolyte) during anodization.

Herein, the anodization in NaHCO<sub>3</sub> electrolyte is carried out for the first time stirring the Zn electrode under controlled conditions at different rotation speed. The aim of this work is to study how different hydrodynamic conditions during the anodization affect the ZnO nanostructures morphology, structure and photoelectrocatalytic behavior for photoelectrochemical water splitting.

## 2. Experimental procedure

Anodization under hydrodynamic conditions was performed in a 2- electrode cell with a rotating disk electrode (RDE) configuration and a platinum foil ( $1 \text{ cm}^2$ ) as the counter electrode. Prior to anodization, Zn rods (99.999% purity) of 8 mm diameter were abraded with 240- 4000 silicon carbide (SiC) grinding papers in order to obtain a mirror finish. Afterwards, they were sonicated for one minute in ethanol and dried in an air stream. Then, the side walls of the zinc rods were coated with Teflon to expose a fixed area of  $0.5 \text{ cm}^2$  to the electrolyte and were anodized in a freshly 50 mM  $\text{NaHCO}_3$  electrolyte at the potential of 10 V for 10 minutes. During anodization, the current density vs. time was registered. Finally, the as-anodized samples were annealed at a temperature of  $300 \text{ }^\circ\text{C}$  (rate of  $15 \text{ }^\circ\text{C/s}$ ) for 1 hour in air.

In order to evaluate the crystalline structure, as-anodized and annealed samples were examined by confocal Raman spectroscopy (Witec Raman Confocal microscope). For these measurements the samples were illuminated by 488 nm neon laser. The morphology of the ZnO annealed samples was also analyzed by using a field emission scanning electron microscope (FE-SEM).

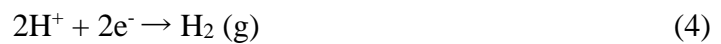
The electrochemical and photoelectrochemical water splitting behavior of the nanostructures was evaluated under simulated sunlight condition AM 1.5 ( $100 \text{ mW/cm}^2$ ) in different solutions. The results in  $\text{Na}_2\text{S}/\text{Na}_2\text{SO}_3$  solution will be presented in this work due to its effectiveness, as it will be explained later. For these experiments, a 3-electrode cell configuration was used, where the ZnO nanostructure (with an effective area of  $0.26 \text{ cm}^2$ ) was the working electrode (photoanode), a saturated Ag/AgCl (3M KCl) the reference electrode and a platinum tip the counter electrode. Photocurrent vs. applied potential were recorded by chopped light radiation (60 s in the dark and 20 s under

illumination) while scanning the potential from -1.00 V to +0.70 V with a rate of 2 mV/s using a potentiostat.

### 3. Results and discussions

#### 3.1. Current density transients during anodization

Figure 1 shows the current density transients during anodization of Zn in NaHCO<sub>3</sub> 50 mM at 10 V for 10 minutes at 0 and from 1000 to 5000 rpm. Under stagnant conditions the current density decreases gradually. This seems to be the result of the formation of a layer covering the surface of the electrode. Under hydrodynamic conditions three stages are observed. That is in line with that reported by Mah et al. [20]. In the first seconds of anodization (stage I) a rapid rise of the current density is observed corresponding to the Zn oxidation to Zn<sup>2+</sup> (eq.1). Afterwards, the current density remains almost constant (stage II) due to the steady state between Zn dissolution and nanostructures formation by precipitation. Some authors suggested the latter corresponds to the hydrolyzation of Zn<sup>2+</sup> to form hydroxyl complex (due to the basic pH) that in presence of HCO<sub>3</sub><sup>-</sup> ions forms hydrozincite (eq. 2 and 3) [2][20], while in the cathode the protons produce hydrogen gas (eq.4). Eventually, current density decays (stage III) since the surface results completely covered by nanostructures that hinder charge transfer.



During anodization in hydrodynamic conditions, due to RDE rotation, the electrolyte is driven from the bulk towards the electrode surface along y-axis and perpendicular to it, and owing to centrifugal force, the electrolyte is thrown radially from the centre of the

electrode outwards [23]. Thus, hydrodynamic conditions may influence the growth of nanowires in two opposite ways: on the one hand, they may remove dissolved zinc near electrode surface and consequently, decrease nanowires growth rate by precipitation; on the other hand, they may improve mass transfer toward electrode surface and as a result, promote the presence of soluble species responsible of nanowires formation [24].

In figure 1 it is noteworthy that at higher rotation speed the constant current density of the stage II extends longer in time and the drop in the current density of the region III takes place later. This indicates that the first factor had more influence on nanowires formation, in which at higher rotation speeds dissolved zinc is removed from the surface of the electrode and the conditions that produce precipitation of the nanostructures over the surface are reached later, delaying the time in which the surface of the electrode is completely covered by nanostructures.

After the anodization process a thermal annealing is performed in order to carry out the conversion of the hydrozincite to ZnO following the suggested reaction of decomposition shown in eq. 5 [2,20].



### **3.2. Raman spectroscopy characterization**

With the purpose of studying the crystallinity and the vibrational properties of the samples and therefore verify the correct formation of wurtzite ZnO crystalline structure, Raman spectroscopy study of as-anodized and annealed electrodes was performed.

The optical phonon modes at Brillouin zone of the ZnO wurtzite structure presents the irreducible representation that follows:  $\Gamma = A_1 + 2B_1 + E_1 + 2E_2$  [5,6,11].  $A_1$  and  $E_2$  modes are both polar and split into transverse optical (TO) and longitudinal optical (LO)

phonons [5,6,11,25]; being Raman and infrared active [6]. Mode B1 is silent [5,11] while E2 has two modes of low (E2 low) and high (E2 high) frequency phonons [25,26] which are related to the Zn sublattice [5,6,11] and oxygen atoms vibration [5,11], respectively.

Figure 2 shows Raman-scattering spectra of as-anodized (a) and annealed (b) electrodes anodized at 0 and 5000 rpm. In both cases a very similar spectrum at 0 and 5000 rpm is obtained. A higher intensity peak for A1, E1 (LO) mode in the annealed electrode anodized at 5000 rpm can be observed at  $\sim 584 \text{ cm}^{-1}$  (fig.2.(b)). This peak is related to oxygen defects, which could explain the increase of the photoluminescence observed in the spectra in comparison with the anodized at 0 rpm. However, it could be said that hydrodynamic conditions during the anodization process does not considerably affect the composition or crystal structure of the electrodes. Figure 2 (c) shows Raman-scattering spectra of as-anodized and annealed samples with the identification markers of the resulting peaks (arrows indicate first order Raman modes for ZnO wurtzite structure, while diamonds indicate the second order and dots the non-related with ZnO peaks). The Raman shift of these peaks and their corresponding theoretical values reported by other authors are collected in Table I.

For the as-anodized sample the highest intensity peak arises at  $1100 \text{ cm}^{-1}$ , associated with the C-OH mode [9]. At  $101 \text{ cm}^{-1}$  a peak associated to E1 (low) ZnO is observed, while at  $704 \text{ cm}^{-1}$ , a low intensity peak is observed that corresponds to the  $\text{CO}_3^{2-}$   $\nu_2$  bending mode. These results are consistent with the generally accepted composition of the as-anodized nanostructures consisting of zinc hydroxycarbonates, hydroxides and oxides [2,3,20].

In the Raman spectra of the annealed sample several peaks corresponding to ZnO wurtzite hexagonal phase are manifested. E2 low and high peaks are observed at  $101 \text{ cm}^{-1}$  and  $438$

$\text{cm}^{-1}$ , respectively. E2 (high) mode corresponds to band characteristic of wurtzite phase [6,9,25,26]. The presence of this peak and its high intensity compared with the other peaks reveal that the annealed electrode presents a ZnO wurtzite hexagonal phase with good crystallinity [25]. Besides, at  $333 \text{ cm}^{-1}$  appears a peak originated from multiple-phonon scattering that corresponds to the second order Raman scattering (E2 (high) - E2 (low)) [9,25], related to Zn-O vibration [9], and a peak at  $202 \text{ cm}^{-1}$  corresponding to  $2\text{TA}/2\text{E2}$  (low).  $2\text{LO}$  peaks at  $\sim 1105 \text{ cm}^{-1}$  and  $1158 \text{ cm}^{-1}$  are arising due to overtone and they also represent the multi-phonon scattering [27]. Peaks at  $380$  and  $410 \text{ cm}^{-1}$  correspond to the TO mode with A1 and E1 symmetry, respectively, while A1 (LO) and E1 (LO) appear at  $573$  and  $584 \text{ cm}^{-1}$ . These LO phonon modes are generally associated with the oxygen vacancies, zinc interstitial defect states and free carriers [6,26,27], therefore its existence confirms some of these defects in the annealed samples. Additionally, a weak Raman peak arise at  $700 \text{ cm}^{-1}$  due to the carbonate [28] residual content of the sample after annealing. Considering the abovementioned, it confirms the successful conversion of the annealed sample to ZnO hexagonal wurtzite structure.

### **3.3. Morphological characterization with FE-SEM images**

The morphological characterization of the annealed samples anodized at different rotation speeds was performed to study the influence of hydrodynamic conditions during anodization on the morphology of the nanostructures. Figure 3 shows FE-SEM images and surface pictures of the ZnO annealed electrodes anodized at  $0 \text{ rpm}$  (left) and  $5000 \text{ rpm}$  (right). It is clearly observed that for the sample anodized under stagnant conditions, the surface does not present uniformity, alternating areas of ordered nanostructures with areas consisting of several mounds of disordered nanostructures; while for the sample

anodized at 5000 rpm the surface is completely homogeneous conforming ordered nanostructures that will be discussed below. The lack of uniformity in stagnant conditions in comparison with hydrodynamic conditions may be the result of a faster localized precipitation of the nanostructures as a result of high concentration of  $Zn^{+2}$  ions nearby zinc is dissolved, while when stirring the electrode,  $Zn^{+2}$  ions are distributed over the surface of the electrode due to the hydrodynamic flux, as it was explained before. Besides, during anodization in stagnant conditions hydrogen bubbles coming from the cathode (Pt) were observed over the anode surface (Zn), while they were eliminated by stirring the electrode. They could affect the ordered growth of the nanostructures promoting the formation of holes and cracks.

Figure 4 shows FE-SEM images at 1000X (left) and 5000X (right) of the annealed ZnO nanostructures anodized from 0 to 5000 rpm. It can be observed that the resulting nanostructures at 0 rpm are conformed by a tangle of nanowires with different thickness. When the rotation speed during anodization is increased, the area occupied by these non-ordered region decreases; while at the same time, the area occupied by ordered regions increases covering the whole surface of the electrode at 3000 rpm and higher rotation velocities. These nanostructures consist of ordered nanowires (about 11-18  $\mu m$  in length) growing from the same point with the structure of flowers. At higher rotation speeds the growth of the nanowires is slower and consequently more organized, due to the removal and distribution over the electrode surface of the dissolved zinc and other species responsible of nanowires formation.

Figure 5 depicts a magnification of the images, in which the centre of the flowers is shown, to observe the thickness of the nanowires formed at 3000 (a), 4000 (b) and 5000 (c) rpm. It can be appreciated that the thickness of the nanowires at 5000 rpm is lower than for the others: the samples anodized at 3000 rpm and 4000 rpm present average

diameters of 147 and 142 nm, respectively, while the one anodized at 5000 rpm 67 nm. Additionally, the diameter of the nanowires was observed to present uniformity along the wire, except just at the tip, where it gets thinner.

### **3.4. Photoelectrochemical water splitting measurements**

Photoelectrochemical water splitting measurements using ZnO nanostructures as photoanodes were carried out in different solutions. 0.5 M Na<sub>2</sub>SO<sub>3</sub> and 0.5 M Na<sub>2</sub>SO<sub>4</sub> were not appropriate because ZnO electrodes undergo photocorrosion, while with 0.1 M NaOH the photoelectrochemical response observed was too low. Therefore, it was decided to employ a sacrificial polysulfide electrolyte consisting of a solution of 0.24 M Na<sub>2</sub>S and 0.35 M Na<sub>2</sub>SO<sub>3</sub> [9].

Figure 6 shows the current density with respect to the applied potential of the photoelectrochemical water splitting experiment for the different ZnO nanostructures under light on/off conditions. It can be appreciated that the nanostructure at 0 rpm presents the highest value of dark current density, generally associated with electrochemical degradation of the electrode [9]. This value decreases gradually as increases rotation velocity during anodization from 0-3000 rpm, while it does not experiment major variations between 3000-5000 rpm. Observing FE-SEM images, it is seen that the dark current values are related somehow to the grade of homogeneity of the sample, meaning that areas of disordered nanostructures in the photoanodes provide higher values in dark current, which decrease and finally stabilize when the ordered nanowires homogeneously cover the whole surface of the photoanode (at 3000 rpm and higher). This could indicate that metallic zinc electrochemical response could contribute, as well, in the increase of dark current density values, since holes and cracks on the surface of the electrode could

be easily photodegraded and would leave small parts of the substrate directly in contact with the electrolyte, that would enhance the dark current density values. Additionally, it is important to point out that low dark current values at rotation speeds higher than 3000 rpm indicates a considerably improvement of the photocorrosion resistance of the nanostructures, especially in the potential range between - 0.5 to 0.4 V<sub>Ag/AgCl</sub>.

Additionally, when light is on, the photocurrent density sharply rises, therefore a good photosensitivity is shown for all the nanostructures, indicating good carrier transport properties. Table II shows the photocurrent density response values ( $\Delta i$  (mA/cm<sup>2</sup>), calculated as the absolute photocurrent density minus dark current density) of the different nanostructures at -0.46 V<sub>Ag/AgCl</sub>. It is observed that at 0 rpm a photoelectrochemical response of 0.17 mA/cm<sup>2</sup> is obtained, while it decreases in the anodized at 1000 rpm until 0.09 mA/cm<sup>2</sup>. Under 2000 rpm and at higher electrode rotation speeds the photocurrent is increased again between 0.17 and 0.21 mA/cm<sup>2</sup> reaching the highest value of 0.27 mA/cm<sup>2</sup> at 5000 rpm. In figure 4 (left side), it can be observed that the distribution of the nanostructures over the surface of the electrode is different at 0, 1000 and 2000 rpm between themselves and in comparison with the anodized at 3000, 4000 and 5000 rpm, for which is quite similar. These differences in the electrodes surface should affect, in part, in the photocurrent response. Besides, at 5000 rpm enhancement of crystallinity (sharply E2 (high) Raman peak) and the increase of the oxygen defects (associated with 584 cm<sup>-1</sup> peak in fig. 2(b)) in comparison with the electrode anodized in stagnant conditions were observed in Raman spectra, that could also improve the photocurrent response [29]. Furthermore, although the distribution of the nanostructures in the samples anodized at 3000, 4000 and 5000 rpm is quite similar, a thinner diameter of the nanowires was observed in the sample anodized at 5000 rpm (see fig. 5). This could explain the higher values in photocurrent response since a thinner diameter of the

nanowires would increase the surface-to-volume ratio improving light absorption [19]. Considering the low value of dark current and highest photocurrent density response, the best nanostructure for water splitting is the anodized at 5000 rpm.

#### 4. Conclusions

In the present study, ZnO nanostructures were synthesized by a rapid and simple anodization method varying the electrode rotation speed under controlled conditions (from 0 to 5000 rpm) in NaHCO<sub>3</sub> electrolytes followed by thermal annealing. Raman spectroscopy confirmed that after the anodization the nanostructures were composed of hydroxycarbonates, hydroxides and oxides which were converted successfully after annealing to crystalline wurtzite ZnO.

The morphology of the nanostructures was observed to be influenced by hydrodynamic conditions during the anodization. Under stagnant conditions, the samples presented a poor uniformity in the distribution of the nanostructures over the surface, while when the rotation speed was increased the homogeneity was improved at 3000 rpm and higher values, from which a completely homogeneous surface with ordered high surface-to-volume ratio nanowires with the structure of flowers was achieved. In addition, in the anodization at 5000 rpm, thinner nanowires for the electrodes were yielded.

The ZnO nanostructures presented high photocurrent density response during water splitting experiments in aqueous Na<sub>2</sub>S/Na<sub>2</sub>SO<sub>3</sub> electrolyte, especially the sample anodized at 5000 rpm which presented an improvement of the 159% in the photocurrent density response with respect to the anodized under stagnant conditions. Rotation speeds higher than 3000 rpm during anodization resulted in a sharp decrease of dark current densities during water splitting test. Therefore, using rotation speeds higher than 3000 rpm during anodization, provide stable and photosensitive ZnO nanostructures, which were successfully used as a photocatalyst for photoelectrochemical water splitting.

## **Acknowledgements**

Authors would like to express their gratitude for the financial support to the Generalitat Valenciana and to the European Social Fund within the subvention to improve formation and employability of technical and management staff of I+D (GJIDI/2018/A/067) and for its financial support through the project: IDIFEDER/018/044. Authors also thank for the financial support to the Ministerio de Economía y Competitividad (Project Code: CTQ2016-79203-R), for its help in the Laser Raman Microscope acquisition (UPOV08-3E-012) and for the co-finance by the European Social Fund. Ramón M. Fernández Domene also thanks the UPV for the concession of a post-doctoral grant (PAID-10-17).

## References

- [1] Y.H. Chen, Y.M. Shen, S.C. Wang, J.L. Huang, Fabrication of one-dimensional ZnO nanotube and nanowire arrays with an anodic alumina oxide template via electrochemical deposition, *Thin Solid Films*. 570 (2014) 303–309. doi:10.1016/j.tsf.2014.03.014.
- [2] L. Zaraska, K. Mika, K. Syrek, G.D. Sulka, Formation of ZnO nanowires during anodic oxidation of zinc in bicarbonate electrolytes, *J. Electroanal. Chem.* 801 (2017) 511–520. doi:10.1016/j.jelechem.2017.08.035.
- [3] L. Zaraska, K. Mika, K.E. Hnida, M. Gajewska, T. Łojewski, M. Jaskuła, G.D. Sulka, High aspect-ratio semiconducting ZnO nanowires formed by anodic oxidation of Zn foil and thermal treatment, *Mater. Sci. Eng. B Solid-State Mater. Adv. Technol.* 226 (2017) 94–98. doi:10.1016/j.mseb.2017.09.003.
- [4] J. Zhao, X. Wang, J. Liu, Y. Meng, X. Xu, C. Tang, Controllable growth of zinc oxide nanosheets and sunflower structures by anodization method, *Mater. Chem. Phys.* 126 (2011) 555–559. doi:10.1016/j.matchemphys.2011.01.028.
- [5] A.Y. Faid, N.K. Allam, Stable solar-driven water splitting by anodic ZnO nanotubular semiconducting photoanodes, *RSC Adv.* 6 (2016) 80221–80225. doi:10.1039/c6ra18747a.
- [6] S. He, M. Zheng, L. Yao, X. Yuan, M. Li, L. Ma, W. Shen, Preparation and properties of ZnO nanostructures by electrochemical anodization method, *Appl. Surf. Sci.* 256 (2010) 2557–2562. doi:10.1016/j.apsusc.2009.10.104.
- [7] A. Kolodziejczak-Radzimska, T. Jesionowski, Zinc oxide—from synthesis to application: A review, *Materials (Basel)*. 7 (2014) 2833–2881. doi:10.3390/ma7042833.
- [8] L. Atourki, E.H. Ihalane, H. Kirou, K. Bouabid, A. Elfanaoui, L. Laanab, X. Portier, A. Ihlal, Characterization of nanostructured ZnO grown by linear sweep voltammetry, *Sol. Energy Mater. Sol. Cells*. 148 (2016) 20–24. doi:10.1016/j.solmat.2015.10.003.
- [9] R. Sánchez-Tovar, R.M. Fernández-Domene, M.T. Montañés, A. Sanz-Marco, J. Garcia-Antón, ZnO/ZnS heterostructures for hydrogen production by photoelectrochemical water splitting, *RSC Adv.* 6 (2016) 30425–30435. doi:10.1039/c6ra03501a.
- [10] A. Kushwaha, M. Aslam, ZnS shielded ZnO nanowire photoanodes for efficient water splitting, *Electrochim. Acta*. 130 (2014) 213–221. doi:10.1016/j.electacta.2014.03.008.
- [11] M.C. Huang, T. Wang, B.J. Wu, J.C. Lin, C.C. Wu, Anodized ZnO nanostructures for photoelectrochemical water splitting, *Appl. Surf. Sci.* 360 (2016) 442–450. doi:10.1016/j.apsusc.2015.09.174.
- [12] Y. Ji, One-step method for growing of large scale ZnO nanowires on zinc foil, *Mater. Lett.* 138 (2015) 92–95. doi:10.1016/j.matlet.2014.09.095.

- [13] L. Liu, W. Wang, J. Long, S. Fu, Y. Liang, J. Fu, Three-dimensional plasmonic photoanode of Au nanoparticles/ZnFe<sub>2</sub>O<sub>4</sub> nanosheets coated onto ZnO nanotube arrays for photoelectrochemical production of hydrogen, *Sol. Energy Mater. Sol. Cells*. 195 (2019) 330–338. doi:10.1016/j.solmat.2019.03.028.
- [14] C. Florica, N. Preda, A. Costas, I. Zgura, I. Enculescu, ZnO nanowires grown directly on zinc foils by thermal oxidation in air: Wetting and water adhesion properties, *Mater. Lett.* 170 (2016) 156–159. doi:10.1016/j.matlet.2016.02.035.
- [15] A. Achour, M.A. Soussou, K. Ait Aissa, M. Islam, N. Barreau, E. Faulques, L. Le Brizoual, M.A. Djouadi, M. Boujtita, Nanostructuring and band gap emission enhancement of ZnO film via electrochemical anodization, *Thin Solid Films*. 571 (2014) 168–174. doi:10.1016/j.tsf.2014.10.061.
- [16] J. Park, K. Kim, J. Choi, Formation of ZnO nanowires during short durations of potentiostatic and galvanostatic anodization, *Curr. Appl. Phys.* 13 (2013) 1370–1375. doi:10.1016/j.cap.2013.04.015.
- [17] C.H. Hsu, D.H. Chen, Photoresponse and stability improvement of ZnO nanorod array thin film as a single layer of photoelectrode for photoelectrochemical water splitting, *Int. J. Hydrogen Energy*. 36 (2011) 15538–15547. doi:10.1016/j.ijhydene.2011.09.046.
- [18] L. De Marco, D. Calestani, A. Quattieri, R. Giannuzzi, M. Manca, P. Ferro, G. Gigli, A. Listorti, R. Mosca, Single crystal mesoporous ZnO platelets as efficient photoanodes for sensitized solar cells, *Sol. Energy Mater. Sol. Cells*. 168 (2017) 227–233. doi:10.1016/j.solmat.2017.04.001.
- [19] A. Sanz-Marco, R. Sánchez-Tovar, M.M. Bajo, R.M. Fernández-Domene, J. García-Antón, Cathodoluminescence characterization of ZnO/ZnS nanostructures anodized under hydrodynamic conditions, *Electrochim. Acta*. 269 (2018) 553–559. doi:10.1016/j.electacta.2018.03.046.
- [20] C.F. Mah, K.P. Beh, F.K. Yam, Z. Hassan, Rapid Formation and Evolution of Anodized-Zn Nanostructures in NaHCO<sub>3</sub> Solution, *ECS J. Solid State Sci. Technol.* 5 (2016) M105–M112. doi:10.1149/2.0061610jss.
- [21] A.Y. Faid, N.K. Allam, Stable solar-driven water splitting by anodic ZnO nanotubular semiconducting photoanodes, *RSC Adv.* 6 (2016) 80221–80225. doi:10.1039/c6ra18747a.
- [22] R. Sánchez-Tovar, K. Lee, J. García-Antón, P. Schmuki, Formation of anodic TiO<sub>2</sub> nanotube or nanosponge morphology determined by the electrolyte hydrodynamic conditions, *Electrochem. Commun.* 26 (2013) 1–4. doi:10.1016/j.elecom.2012.09.041.
- [23] A.J. Bard, L.R. Faulkner, *Electrochemical Methods: Fundamentals and Applications*, 2001.
- [24] R.M. Fernández-Domene, R. Sánchez-Tovar, E. Segura-Sanchís, J. García-Antón, Novel tree-like WO<sub>3</sub> nanoplatelets with very high surface area synthesized by anodization under controlled hydrodynamic conditions, *Chem. Eng. J.* 286 (2016) 59–67. doi:10.1016/j.cej.2015.10.069.

- [25] A. Khan, N. Sciences, Raman Spectroscopic Study of the ZnO Nanostructures Raman Spectroscopic Study of the ZnO Nanostructures, *J Pak Mater Soc.* 4 (1) (2010) 5–9.
- [26] A.K. Bhunia, P.K. Jha, D. Rout, S. Saha, Morphological Properties and Raman Spectroscopy of ZnO Nanorods, *J. Phys. Sci.* 21 (2016) 111–118. [www.vidyasagar.ac.in/journal](http://www.vidyasagar.ac.in/journal).
- [27] R. Ghosh, S. Kundu, R. Majumder, M.P. Chowdhury, Hydrothermal synthesis and characterization of multifunctional ZnO nanomaterials, *Mater. Today Proc.* (2019). doi:10.1016/j.matpr.2019.04.217.
- [28] R.L. Frost, A. López, L. Wang, R. Scholz, N.P. Sampaio, SEM, EDX and Raman and infrared spectroscopic study of brianyoungite  $Zn_3(CO_3,SO_4)(OH)_4$  from Esperanza Mine, Laurion District, Greece, *Spectrochim. Acta - Part A Mol. Biomol. Spectrosc.* 149 (2015) 279–284. doi:10.1016/j.saa.2015.04.013.
- [29] N.K. Shrestha, K. Lee, R. Hahn, P. Schmuki, Corrigendum to ‘Anodic growth of hierarchically structured nanotubular ZnO architectures on zinc surfaces using a sulfide based electrolyte’ [*Electrochemistry Communications* 34 (2013) 9–13], *Electrochem. Commun.* 34 (2013) 361. doi:10.1016/j.elecom.2013.07.003.
- [30] S. Guo, X. Zhao, W. Zhang, W. Wang, Materials Science & Engineering B Optimization of electrolyte to significantly improve photoelectrochemical water splitting performance of ZnO nanowire arrays, *Mater. Sci. Eng. B.* 227 (2018) 129–135. doi:10.1016/j.mseb.2017.09.020.
- [31] L.A. R. Cuscó, E.A. Lladó, J. Ibáñez, Temperature dependence of Raman scattering in ZnO, *Phys. Rev. B.* 75 (2007) 165202 1–11. doi:10.1103/PhysRevB.75.165202.

**Table I.** Experimental Raman shift ( $\text{cm}^{-1}$ ) of the identified peaks in the Raman spectra for the as-anodized and annealed samples; symmetry and theoretical (theor.) values given by other authors and their references.

Raman shift ( $\text{cm}^{-1}$ )		Symmetry	Theor. ( $\text{cm}^{-1}$ )	Marker	Ref.
as-anodized	annealed				
101	101	wurtzite ZnO E2 (low)	~100	↓	[6,22,30]
	202	wurtzite ZnO 2TA; 2E2 (low)	~203	◇	[9,11]
390	335	wurtzite ZnO E2(high)-E2(low)	333		[9]
	378	wurtzite ZnO A1(TO)	~380		[6,22,25]
	410	wurtzite ZnO E1(TO)	410		[6,9]
	438	wurtzite ZnO E2(high)	~438	↓	[6,11]
	573	wurtzite ZnO A1(LO)	~573		[6,10,30]
	584	wurtzite ZnO E1(LO)	~584		[6,30]
704	704	Carbonate group $\nu_2$	706	•	[27]
1100		C-OH	1100		[9]
	1105	wurtzite ZnO 2LO	~1105		[26]
	1158	wurtzite ZnO 2A1(LO),2E1(LO);2LO	1158	◇	[31]

**Table II.** Photocurrent response in Na<sub>2</sub>S/Na<sub>2</sub>SO<sub>3</sub> solution for the different nanostructures at -0.46 V<sub>Ag/AgCl</sub> of applied potential.

Rpm	$\Delta i$ (mA/cm <sup>2</sup> )
0	0.17
1000	0.09
2000	0.18
3000	0.17
4000	0.21
5000	0.27

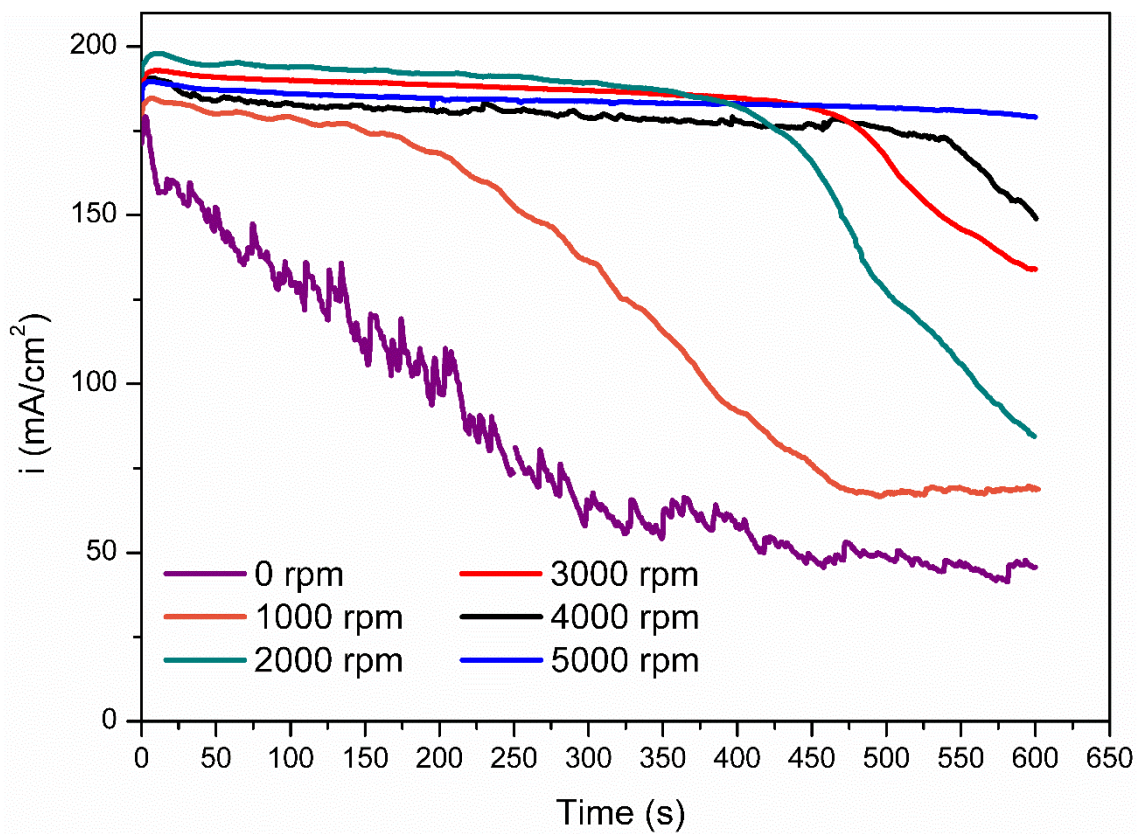


**Figure 1.** Current density transients during anodization in 50 mM NaHCO<sub>3</sub> electrolyte at 10 V for 10 minutes at different rpm.

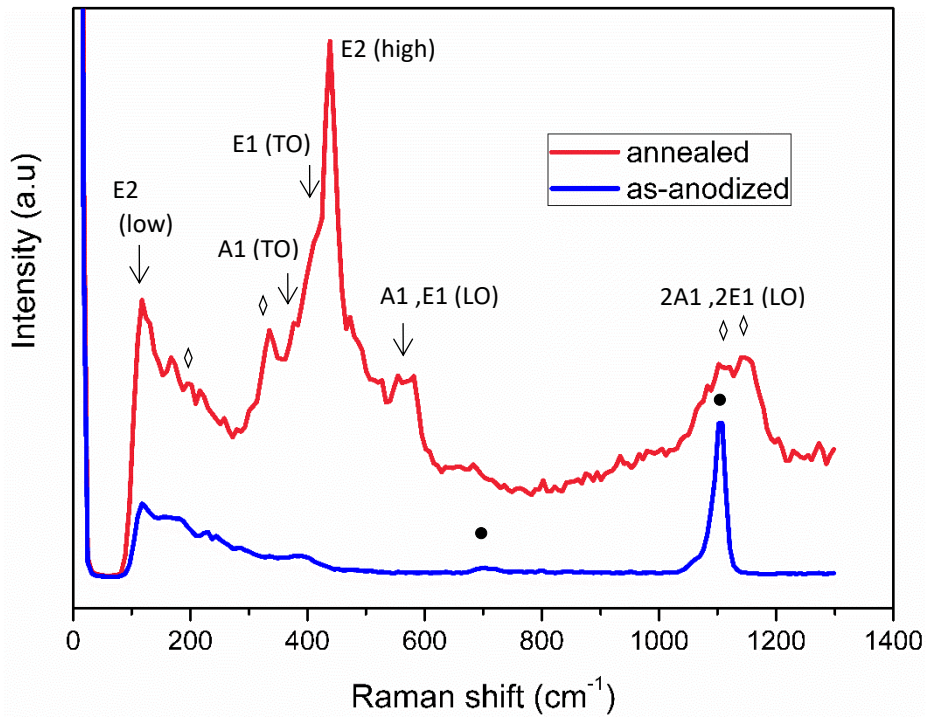


**Figure 2.** Raman spectra of the as-anodized (a) and annealed (b) samples at 0 rpm and 5000 rpm rotation speed, and Raman spectra with identifying markers (c) for the as-anodized (blue) and annealed (pink) samples.

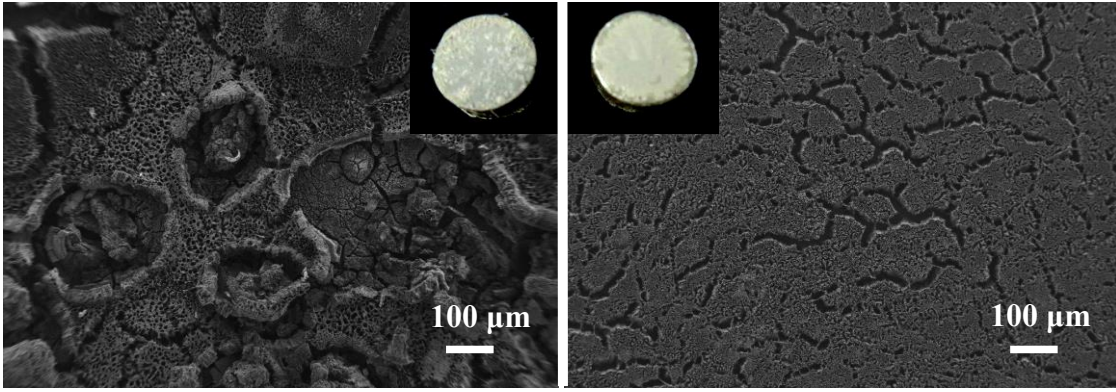


**Figure 3.** FE-SEM images and inset pictures of the samples anodized at 0 rpm (left) and 5000 rpm (right).

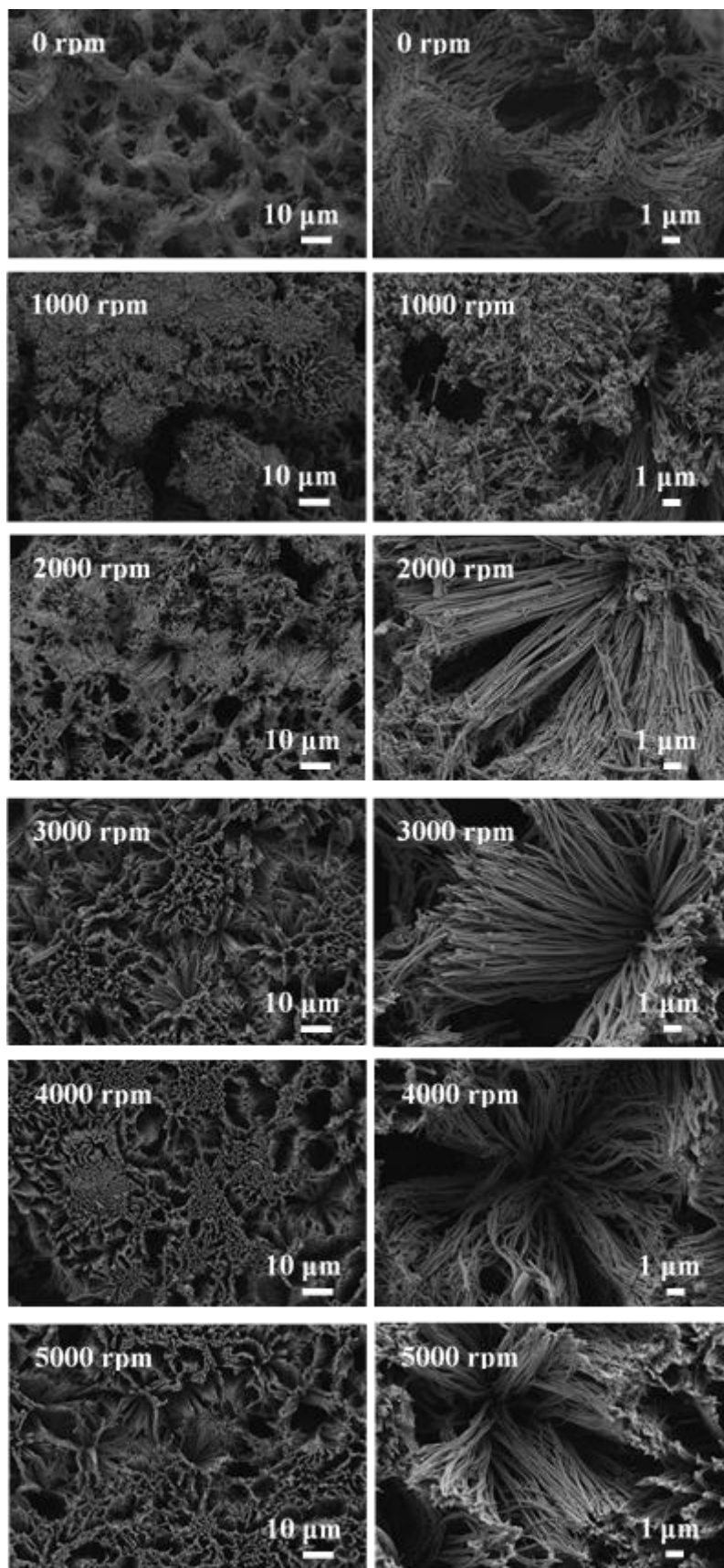


**Figure 4.** FE-SEM images of the samples anodized from 0 to 5000 rpm.

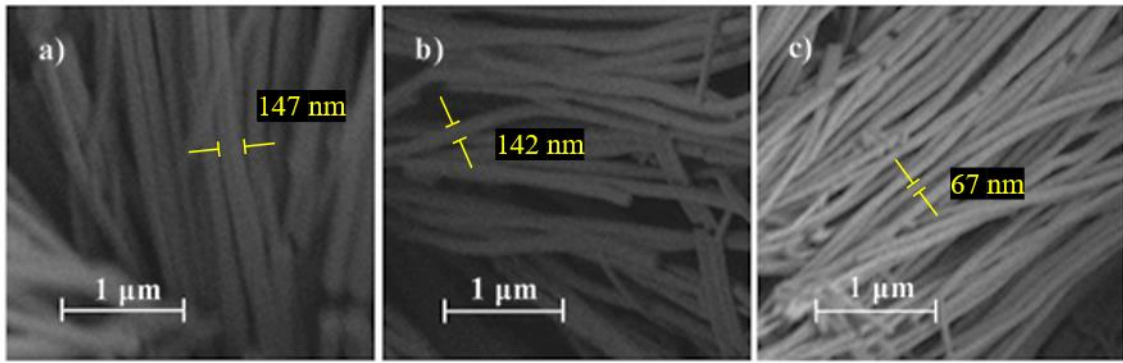


**Figure 5.** Magnification of the FE-SEM images of the samples anodized at 3000 rpm (a), 4000 rpm (b) and 5000 rpm(c) and average diameter of the nanowires for each sample.

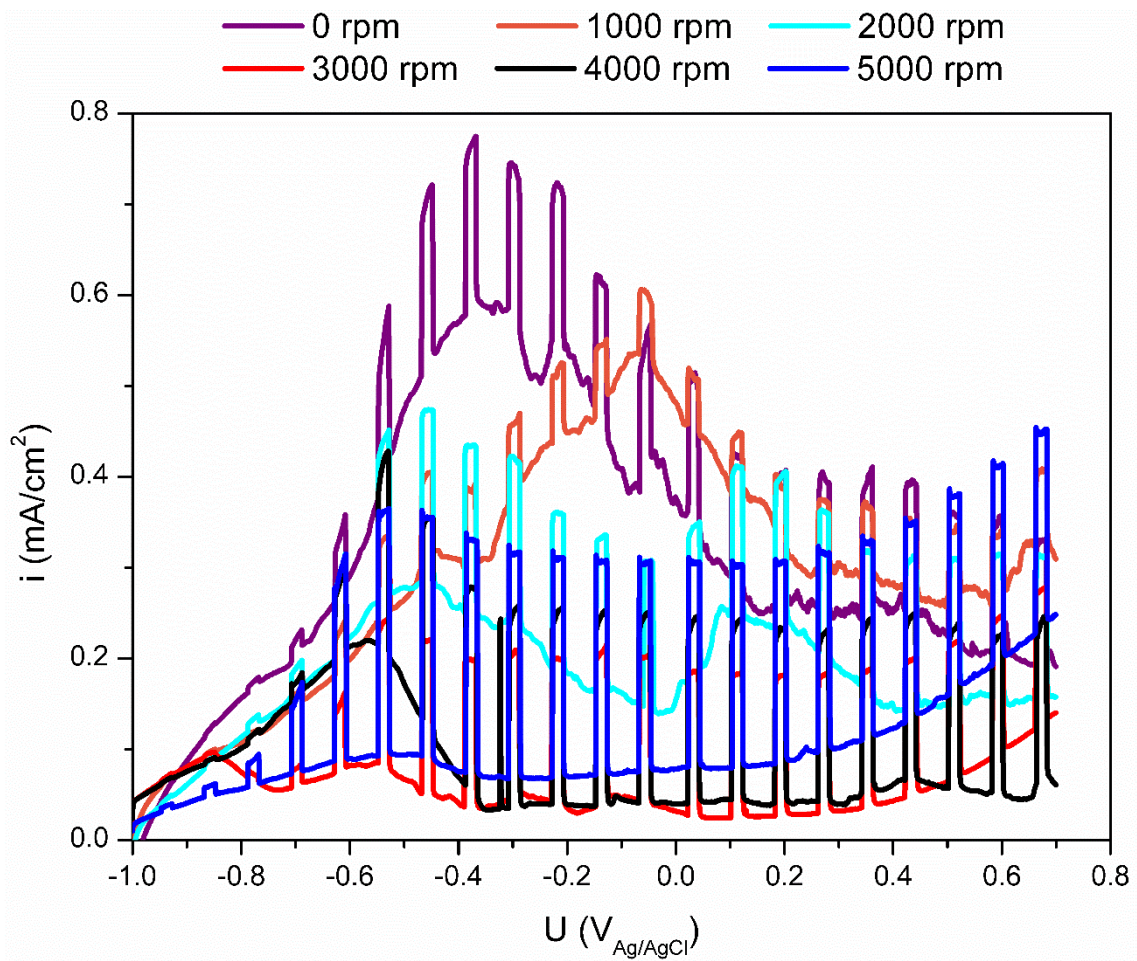


**Figure 6.** Current density under on/off simulated sunlight AM 1.5 conditions in  $\text{Na}_2\text{S}/\text{Na}_2\text{SO}_3$  solution as a function of the applied potential for the nanostructures anodized at different rotation speeds.